Incorporating hydrothermal liquefaction into wastewater treatment – Part II: Characterization, environmental impacts, and potential applications of hydrochar

Huan Liu, Nathalie Lyczko, Ange Nzihou, Cigdem Eskicioglu

Incorporating hydrothermal liquefaction into wastewater treatment – Part II: Characterization, environmental impacts, and potential applications of hydrochar

Huan Liu [a], Nathalie Lyczko [b], Ange Nzihou [b,c,d], Cigdem Eskicioglu [a,*]

[a] UBC Bioreactor Technology Group, School of Engineering, The University of British Columbia, Okanagan Campus, 1137 Alumni Avenue, Kelowna, British Columbia, V1V 1V7, Canada
[b] Université de Toulouse, IMT Mines Albi, RAPSODEE CNRS UMR 5302, Campus Jarlard, F.81013, Albi Cedex 09, France
[c] Princeton University, School of Engineering and Applied Science, Princeton, NJ, 08544, USA
[d] Princeton University, Andlinger Center for Energy and the Environment, Princeton, NJ, 08544, USA

A B S T R A C T

Hydrothermal liquefaction (HTL) is a promising technique for renewable biofuel (biocrude) production from municipal sludge. However, its solid byproduct, hydrochar, requires sustainable management for further resource recovery and pollution control. This study comprehensively assessed the properties, environmental influences, and possible utilizations of hydrochar generated from mixed sludge (MS). With the increase of HTL reaction temperatures (290–360 °C) and residence time (0–30 min), the dry-weight contents of ash and fuel ratio increased from 10.5% and 0.1 in MS to 48.7–68.5% and 0.4–0.7 in hydrochar, respectively. However, the dry-basis contents of volatile matter, carbon, and higher heating value sharply decreased to 18.7–35.9%, 22.9–37.3%, and 8.6–16.0 MJ/kg, respectively. The leaching risks of inorganic contaminants from hydrochar were limited and controllable in various scenarios. Hydrochar performed more stable combustion than sludge, but its high ash contents and alkali index (0.28–0.72 kg/GJ) implied high risks of slagging and fouling. Hydrochar has a good potential for carbon sequestration due to low O/C ratios (<0.2) and improved recalcitrance index (0.43–0.48). Benefiting from intrinsic metals (e.g., Ca and Fe), catalytic hydrochar graphitization was feasible at a moderate temperature (1200 °C). Although hydrochar was restricted from land application for heavy metals accumulation, it is promising for metals and nutrient recovery. It has a total phosphorus (P) of 7.2–8.5% by weight, and thus P recovery is critical and necessary for mitigating environmental challenges and global P scarcity. Overall, this study contributed to the state-of-the-art in waste-to-resource development and cleaner production.

1. Introduction

Municipal sludge (commonly called sewage sludge) is a semi-solid by-product of municipal wastewater treatment processes. Its high moisture (95–98% by weight, wt%), significant volume, and hazardous contents (e.g., pathogens, organic and inorganic pollutants, and emerging contaminants) are barriers to its proper management (Liu et al., 2021a). Resource recycling and zero waste are becoming primary objectives for sludge handling in the circular economy. Anaerobic digestion has been widely applied to generate methane but is subject to

Abbreviations: AAEMs, alkali and alkaline earth metals; AI, alkali index; ANOVA, analysis of variance; AP, apatite phosphorus; BET, Brunauer–Emmett–Teller; CCD, central composite design; COPCs, constituents of potential concern; db, dry basis; DTG, derivative thermogravimetry; FTIR, Fourier transform infrared spectroscopy; HHV, higher heating value; HTC, hydrothermal carbonization; HTL, hydrothermal liquefaction; IP, inorganic phosphorus; LSP, liquid-solid partitioning; MS, mixed sludge; NAIP, non-apatite inorganic phosphorus; OP, organic phosphorus; SEM, scanning electron microscopy; TCLP, toxicity characteristic leaching procedure; TEM-EDX, transmission electron microscopy with energy dispersive X-ray spectroscopy; TGA, thermogravimetric analysis; TP, total phosphorus; WWTP, wastewater treatment plant; XRD, X-ray diffraction.

* Corresponding author.
E-mail addresses: liu@alumni.ubc.ca (H. Liu), lyczko@mines-albi.fr (N. Lyczko), ange.nzihou@mines-albi.fr (A. Nzihou), cigdem.eskicioglu@ubc.ca (C. Eskicioglu).

low efficiency and requires large land and high capital costs. Land application is often used for digested sludge, but it is becoming less attractive and more expensive due to the contamination of per- and polyfluorinated alkyl substances (PFAS) along with other macro- and micro-contaminants (Johnson, 2022). Incineration is popular in reducing waste volume but has high operating costs for drying process (Đurđević et al., 2019). Hence, the next generation of waste-to-energy technologies is developing. Hydrothermal liquefaction (HTL) is one of the latest options. It utilizes water to create subcritical conditions (280–374 °C and 80–220 bars) and promote ionic reactions, thus efficiently converting biomass into a liquid biofuel (called biocrude) (Liu et al., 2021b). HTL has the advantage to process feedstocks with high moisture (typically 20% solids). Compared to other thermochemical techniques, such as pyrolysis, it can achieve a high biocrude yield and energy recovery without energy-intensive drying (Li et al., 2021). Therefore, HTL is particularly suitable for sludge treatment as a replacement for anaerobic digestion (Basar et al., 2021).

Besides biocrude, HTL generates three by-products, i.e., aqueous phase (wastewater), solid residue (called hydrochar), and gas (mainly CO_2). The biocrude will undergo some upgrading processes (e.g., hydrotreating) to produce liquid transportation fuel. Its characterization and potential upgrading have been well investigated (Heracleous et al., 2022; Liu et al., 2022). The aqueous phase consists of a large amount of process water, with high levels of organic carbon, chemical oxygen demand, ammonium, and toxic compounds (e.g., aromatics and nitrogenous organics) (Watson et al., 2020). Its valorization or management is one of the critical steps for the commercialization of HTL technology. Much effort has been made for the treatment of HTL aqueous, such as anaerobic digestion (Wang et al., 2021a), adsorption (Wang et al., 2022), catalytic hydrothermal gasification (Marrone et al., 2018), wet oxidation (Silva Thomsen et al., 2022), etc. In contrast, hydrochar received much less attention as its quantity is significantly reduced for minimal disposal costs. Although in small amounts, hydrochar is concentrated with resources (e.g., carbon and phosphorus) and constituents of potential concern (COPCs), which requires sustainable management and resource recovery.

Hydrochar is mainly studied as a solid biofuel from the hydrothermal carbonization (HTC) process, typically performed at a low temperature (180–280 °C), while HTL hydrochar received less attention (Liu et al., 2021a). HTL hydrochar is different from HTC hydrochar for the separation of most organics (biocrude) from solids by solvent extraction after cooling in a batch scale or filtration at high temperatures in a continuous plug-flow reactor (Basar et al., 2021). Therefore, HTL hydrochar contains much lower volatile matter and higher ash (up to 88 wt%) contents (Tong et al., 2021). It could be less feasible for combustion as a result of lower energy density (Devi et al., 2022). The higher reaction temperatures in HTL also lead to the loss of oxygen-functional groups in hydrochar due to enhanced decarboxylation and dehydration reactions (Wang et al., 2019). HTL also promotes decomposition, solubilization, and recombination/repolymerization reactions and thus generates hydrochar with different compositions (Lachos-Perez et al., 2022). Therefore, the differences in HTL hydrochar require more studies to confirm for its valorization.

To date, few reports investigated HTL hydrochar. Its yield could vary between 7 and 60% on a dry basis (db) depending on the feedstock sludge properties and HTL conditions (Chang et al., 2021). For instance, the hydrochar yield from a plug-flow continuous-flow HTL treatment (276–358 °C) of primary, secondary, and digested sludge was 9.5, 20.5, and 35.4%, db, respectively (Marrone et al., 2018). Silva Thomsen et al. (2020) reported that HTL could destroy most pharmaceuticals and biocides with undetectable amounts (<10 ppb) remaining in hydrochar. Chang et al. (2021) found that total/leachable contents of PAHs were reduced with lower toxicity in hydrochar compared to sludge. Many studies have concluded that most inorganics are concentrated in hydrochar from sludge, especially Al (3–11%, db), Ca (1–7%, db), Fe (1–10%, db), and P (2–6%, db), enhancing their recovery potential (Liu et al., 2021b). P is listed as a Critical Raw Material by European Union, and its recovery and recycling from waste streams have attracted much attention. However, the accumulation of heavy metals or COPCs is the primary concern for direct recycling of hydrochar in land application. Although some reports suggested the reduced leachability of heavy metals using the toxicity characteristic leaching procedure (TCLP), it is limited to landfilling scenario (Shao et al., 2015). Other studies found inhibited bioavailability of heavy metals in hydrochar through sequential extraction procedures established by Tessier and the Community Bureau of Reference (Leng et al., 2014; Yuan et al., 2011). Some also used quantitative risk assessment methods (e.g., geo-accumulation index, ecological risk index assessment, and risk assessment code) and found reduced environmental risks of heavy metals in hydrochar (Chen et al., 2014; Huang et al., 2011; Leng et al., 2014). However, leaching of COPCs could be largely related to environmental conditions. Therefore, a more comprehensive characterization of metal leaching behaviors is necessary for the application of hydrochar in various scenarios. The composition and properties of hydrochar also significantly depend on the HTL reaction conditions and origin of sludge, but few studies carefully characterized hydrochar for its applications (Leng et al., 2015a; Zhang et al., 2018).

As explained above, the characterization of hydrochar from HTL of municipal sludge is very limited and often omitted, and comprehensive and critical investigations are necessary for its sustainable management. This study thoroughly evaluated the characteristics of hydrochar from the following aspects: Composition and functionality, environmental impacts of major contaminants (inorganics), and potential applications. Mixed primary and secondary sludge was used as the HTL feedstock to represent a typical configuration of wastewater treatment plants. Following Part I (Liu et al., 2022) on the optimization of energy recovery using response surface methodology, the effects of HTL reaction temperature (290–360 °C) and residence time (0–30 min) on hydrochar compositions were examined in this study (Part II). The surface functional groups, morphology, and mineralogy were presented. For the environmental assessment, total and TCLP leachable contents of COPCs were measured and compared to applicable regulations. More specifically, pH-dependent tests were performed to assess the leaching behaviors of COPCs within a wide pH range (2–13) and determine the beneficial use conditions (Garrabrants et al., 2021). P speciation is largely affected by the feedstock composition and associated wastewater treatment processes (Liu et al., 2021b) and therefore was evaluated for the selection of P recovery methods. The combustion performance and carbon sequestration potential were investigated by thermogravimetric analysis (TGA). Considering the significant metal contents, the potential of upgrading hydrochar to graphite at a low temperature (1200 °C) by in-situ catalytic effects was assessed for the first time.

2. Materials and methods

2.1. Materials

Mixed sludge (MS) with a volume ratio of 50% thickened screened primary sludge and 50% thickened waste secondary sludge were obtained from Annacis Island Wastewater Treatment Plant (WWTP) (Delta, British Columbia, Canada). The sludge mixing ratio was selected based on the average annual flow in the WWTP. The MS was dewatered to a solids content of 20wt% using centrifugation, which was loaded as the HTL feedstock. After HTL reaction at various temperatures (290–360 °C) and residence time (0–30 min) using a bench-scale 1-L batch reactor (Parr® 4570), hydrochar was extracted, washed by dichloromethane, dried at 105 °C for 24 h, and ground for analysis. The hydrochar yield was expressed in wet basis (hydrochar mass as received over the mass of dewatered MS) and dry basis (hydrochar dry weight divided by feedstock dry weight). Detailed experimental procedures can be found elsewhere (Liu et al., 2022).

2.2. HTL experimental design

The HTL experiments were performed using a two-factorial central composite design (CCD), with eight axial points (in duplicates) and three replicates at the central point. HTL reaction temperature (A) and residence time (B) were selected as independent variables (Table S1). The data were analyzed by response surface methodology. The hydrochar samples were donated as HCT-t where T and t were the reaction temperature and residence time, respectively.

2.3. Characterization of sludge feedstock and hydrochar

The proximate analysis of dried dewatered MS and hydrochar was performed following ISO 18122–2015 (ash) and ISO 18123–2015 (volatile matter). The ultimate analysis (CHNS) was determined using an automatic elemental analyzer (Costech ECS 4010). The higher heating value (HHV) of dried MS and hydrochar was analyzed by a bomb calorimeter (IKA C5000). Particle size distribution was performed by a Malvern Mastersizer 3000 using the wet module. The measurement principals and procedures of the above parameters can be found in the Chapter 2 of Handbook on Characterization of Biomass, Biowaste and Related By-products (Nzihou, 2020). The total inorganic elements were extracted by microwave-assisted acid digestion (EPA 3051A). The TCLP was performed to assess the mobility of COPCs in MS and hydrochar following the EPA 1311. The liquid-solid partitioning (LSP) tests were conducted to evaluate the COPCs release from MS and hydrochar (after HTL) as a function of pH (2–13) at a liquid to solid (L/S) ratio of 10 mL/g-dry (EPA 1313). The extracted elements were determined by an inductively coupled plasma mass spectrometry (ICP-MS, Agilent 8900 Triple Quad). The P species, such as inorganic P (IP), organic P (OP), apatite P (AP), and non-apatite inorganic P (NAIP) were sequentially extracted using the Standards, Measurements and Testing Protocol (González Medeiros et al., 2005) and determined by ascorbic acid method (APHA 4500-P E). Each analysis was completed at least in duplicates.

2.4. Surface properties and mineralogy

MS and hydrochar were degassed at 110 °C for 10 h for the Brunauer–Emmett–Teller (BET) surface area analysis by a 3Flex Surface Characterization Analyzer (Micromeritics) using N_2 gas. The surface functional groups were analyzed by Fourier transform infrared spectroscopy (FTIR, Thermo Scientific Nicolet iS10). The surface morphology and structure were examined by scanning electron microscopy (SEM, Carl Zeiss Ultra 55) and transmission electron microscopy with energy dispersive X-ray spectroscopy (TEM-EDX, JEOL JEM-ARM200F Cold FEG probe Cs corrected). The mineral crystalline structure was identified using X-ray diffraction (XRD, Phillips Panalytical X'pert Pro MPD).

2.5. Thermogravimetric analysis

The combustion behaviors of MS and hydrochar were performed using simultaneous thermogravimetric analysis and differential scanning calorimetry (TGA-DSC, TA Instruments SDT Q600). Approximately 10 mg of dried sample was heated from 30 to 700 °C at 10 °C/min with an air purge rate of 100 mL/min. Experimental data were blank-corrected. The maximum combustion rate temperature (T_m), maximum mass loss (DTG_{max}), and average mass loss (DTG_{mean}) were acquired from derivative thermogravimetry (DTG) curves. The ignition temperature (T_i) and burnout temperature (T_b) were acquired by the intersection method (Lu and Chen, 2015). The combustion index (S) was calculated by Eq. (1) to reflect the overall combustion rate (Sezer et al., 2021). To evaluate the slagging risk during combustion, the alkali index (AI) was estimated using Eq. (2) (Miles et al., 1995).

$$S = \frac{DTG_{max} DTG_{mean}}{T_i^2 T_b} \tag{1}$$

$$AI\ (kg/GJ) = \frac{K_2O\% + Na_2O\%}{HHV(GJ/kg, dry)} \tag{2}$$

To assess the carbon sequestration potential of hydrochar, the recalcitrance index (R_{50}) was calculated using Eq. (3) (Harvey et al., 2012).

$$R_{50} = T_{50,HC} / T_{50,graphite} \tag{3}$$

where $T_{50,\ HC}$ and $T_{50,\ graphite}$ are temperatures of 50% oxidation/volatilization of hydrochar and graphite (886 °C), respectively. After correction by removing water (mass loss before 150 °C) and ash contents (residue at 700 °C), $T_{50,\ HC}$ was obtained from the TG curves (Fig. S1).

2.6. Statistical analysis

Using response surface methodology, analysis of variance (ANOVA) and response surface plots were performed on CCD experimental data by Design-Expert® Version 13. The statistical significance was evaluated at a confidence level of 95% ($p < 0.05$). The accuracy and reliability of the developed polynomial models were assessed by the coefficient of determination (R^2).

3. Results and discussion

3.1. Characterization of hydrochar

3.1.1. Hydrochar production

As shown in Fig. 1a, hydrochar yields from MS were generally low, 13.7–17.3%, db, at HTL conditions, due to the conversion of sludge biomass into biocrude. The increase of HTL temperature from 290 to 360 °C led to the decrease of hydrochar yield, similar to the effects of residence time from 0 to 15 min. However, hydrochar yield increased slightly when residence time was longer than 15 min at 325 °C, probably because of the char-forming reactions, e.g., condensation and polymerization (Tasca et al., 2019). Notably, the dry yield could vary drastically depending on the sludge type (primary, secondary, mixed, or digested sludge) and reactor configuration (batch vs continuous-flow) (Marrone et al., 2018). On the wet basis (dewatered MS), hydrochar yields remained minimum (≤3.5 wt%), which would significantly reduce the sludge disposal cost.

3.1.2. Proximate and ultimate analyses

Fig. 1b and c showed the proximate and ultimate analyses of hydrochar, respectively. Compared to MS, hydrochar had much higher ash contents due to the loss of volatile matter. It seemed that both low and high reaction severities favored the formation of fixed carbon, while the moderate conditions (around 325 °C) facilitated the conversion of biocrude. Fuel ratio was calculated from the content of fixed carbon divided by volatile matter, which increased at higher HTL reaction severities. The fuel ratio was enhanced from 0.1 in MS to up to 0.7 in hydrochar, just below bituminous coal (1–2.5), indicating that hydrochar could have better combustion performance than MS (Kurose et al., 2004). However, considering high ash contents (up to 68.5%, db) in hydrochar and potential ash slagging issues, ash removal would be necessary before using hydrochar as a solid fuel. The elemental compositions of CHNSO and HHV in hydrochar dramatically decreased compared to MS. The C contents were generally below 37%, db. The low N (2.4–4%, db) and S (0.4–0.9%, db) contents could reduce the NO_x and SO_2 emissions. The van Krevelen diagram (Fig. 1d) illustrated that H/C and O/C molar ratios decreased consistently close to coal quality at higher HTL temperature and residence time, mainly caused by dehydration and decarboxylation reactions, while only minor demethylation

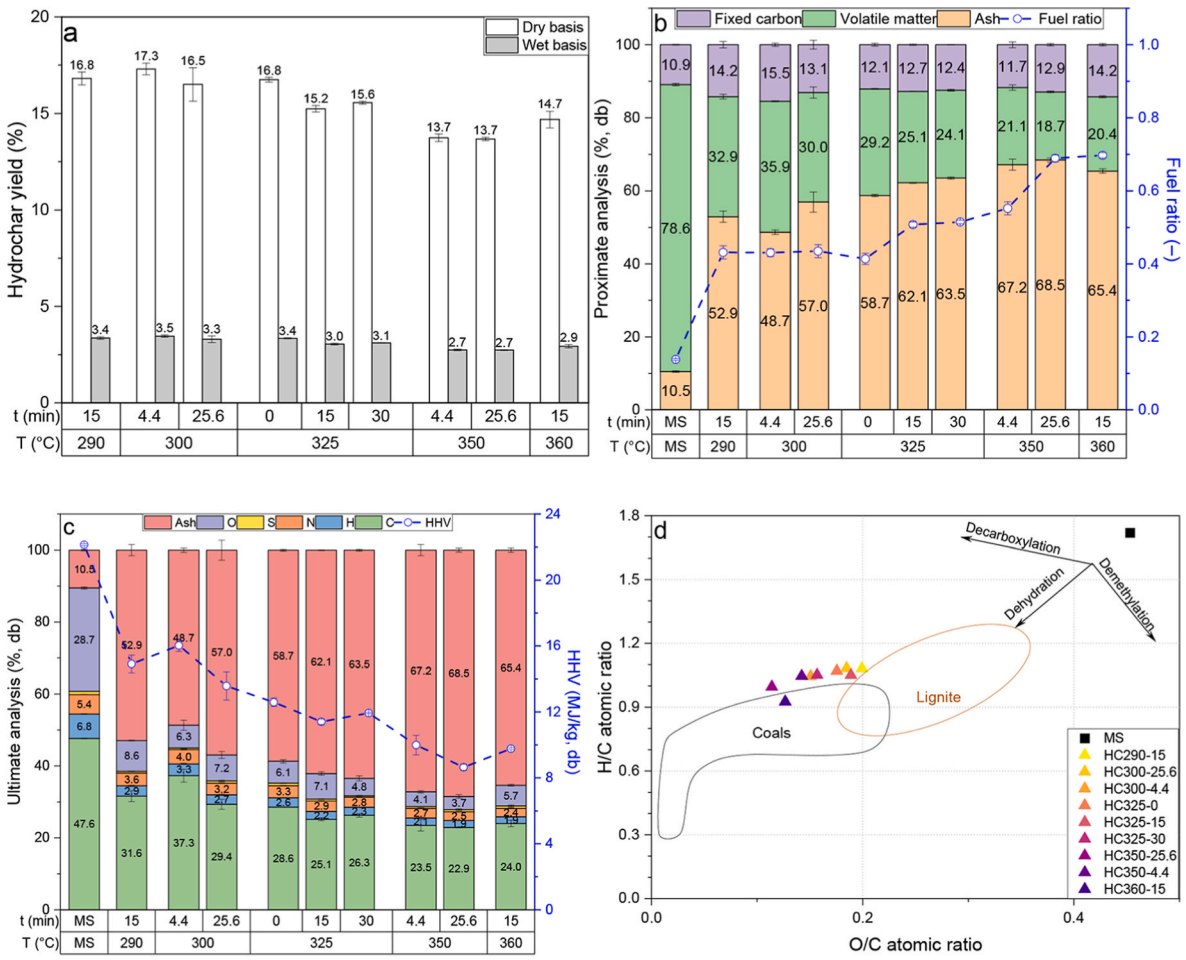

Fig. 1. (a) Yield, (b) proximate analysis, (c) ultimate analysis, and (d) van Krevelen diagram of hydrochar from various HTL reaction temperatures (T) and residence time (t) compared to MS.

(loss of $–CH_3$) occurred during HTL. The hydrochar constituents varied substantially, while the numbers agreed with previously reported ranges for sludge-derived hydrochar (Liu et al., 2021a).

The effects of HTL reaction conditions on hydrochar characteristics were revealed by response surface plots as shown in Fig. 2. Both reaction temperature and residence time showed negative effects on the contents of C, N, volatile matter, and HHV, but positive effects on the ash content and fuel ratio. The enhancement of fuel ratio was mainly contributed by the reduction of volatile matter and/or increase of fixed carbon. Notably, at higher temperatures (e.g., 350 °C), residence time exhibited limited impacts on hydrochar characteristics. The relationship between independent factors and responses was further presented in Eqs. (S1–S6). The response values could be estimated by the actual equations Eqs. (S7–S12). The coded equations suggested that HTL operating conditions had identical effects on C, N, volatile matter, and HHV that were opposite to ash content, suggesting correlations among these responses. Overall, reaction temperature showed more dominant effects than residence time as it determines the decomposition level of biochemical components. Significant interaction effects (AB) were positive for contents of C, N, volatile matter, and fuel ratio but negative for ash, possibly due to the condensed N-containing aromatic compounds from soluble N and carbonyl groups in HTL aqueous phase (Wang et al., 2021b).

The ANOVA in Table S2 indicated that temperature and time were significant ($p < 0.05$) process parameters for most hydrochar properties, while residence time did not significantly affect HHV. The lack of fit values were not significant relative to the pure error, suggesting a good fit of models. The high values of coefficient of determination ($R^2 > 0.9$), adjusted R^2 (>0.8), predicted R^2 (>0.7), and adequate precision (>14) further confirmed the good predictivity of models.

3.1.3. *Surface functional groups*

The FTIR spectra of MS and hydrochar obtained from various HTL conditions were shown in Fig. 3. The band assignments of FTIR are generally classified into organic and inorganic groups and listed in Table S3 (Liu et al., 2021a). Compared to MS, the –OH stretching of hydroxyl groups at 3400–3200 cm^{-1} in hydrochar was weakened due to dehydration reactions. The aliphatic C–H vibration at 3000–2800 cm^{-1} in hydrochar was also less intensive than that of MS, indicating the demethylation or condensation reactions during HTL (Leng et al., 2015a). The peak at around 1620 cm^{-1} was likely a stretching vibration of C–N, which declined due to the decomposition of amino acids after HTL and release of ammonia (He et al., 2016). The occurrence of C═C stretching at 1440 cm^{-1} and out-of-plane aromatic C–H stretching peaks at 800–740 cm^{-1}in hydrochar suggested the formation of aromatic groups. The absent peaks at 1160, 1110, and 1060 cm^{-1} were attributed to the breaking of C–O bond from decarboxylation reactions (Kim et al., 2014). Considering the high contents of P and Fe, the addition of a strong wide band at 1200–1000 cm^{-1} and peaks at 600–470 cm^{-1} in hydrochar were probably related to $–PO_4$ and asymmetric Fe–O (or bending vibrations of Si–O–Fe), respectively (Yu et al., 2019). No significant difference (only slight changes in peak intensity) was observed in FTIR of hydrochar produced at different temperatures or residence time. Overall, hydrochar showed decreased intensity of oxygenated groups and increased intensity of aromatic groups compared to the feedstock. Such improvement is beneficial to C sequestration, C stability, and surface activity, showing potential for water and nutrient retention

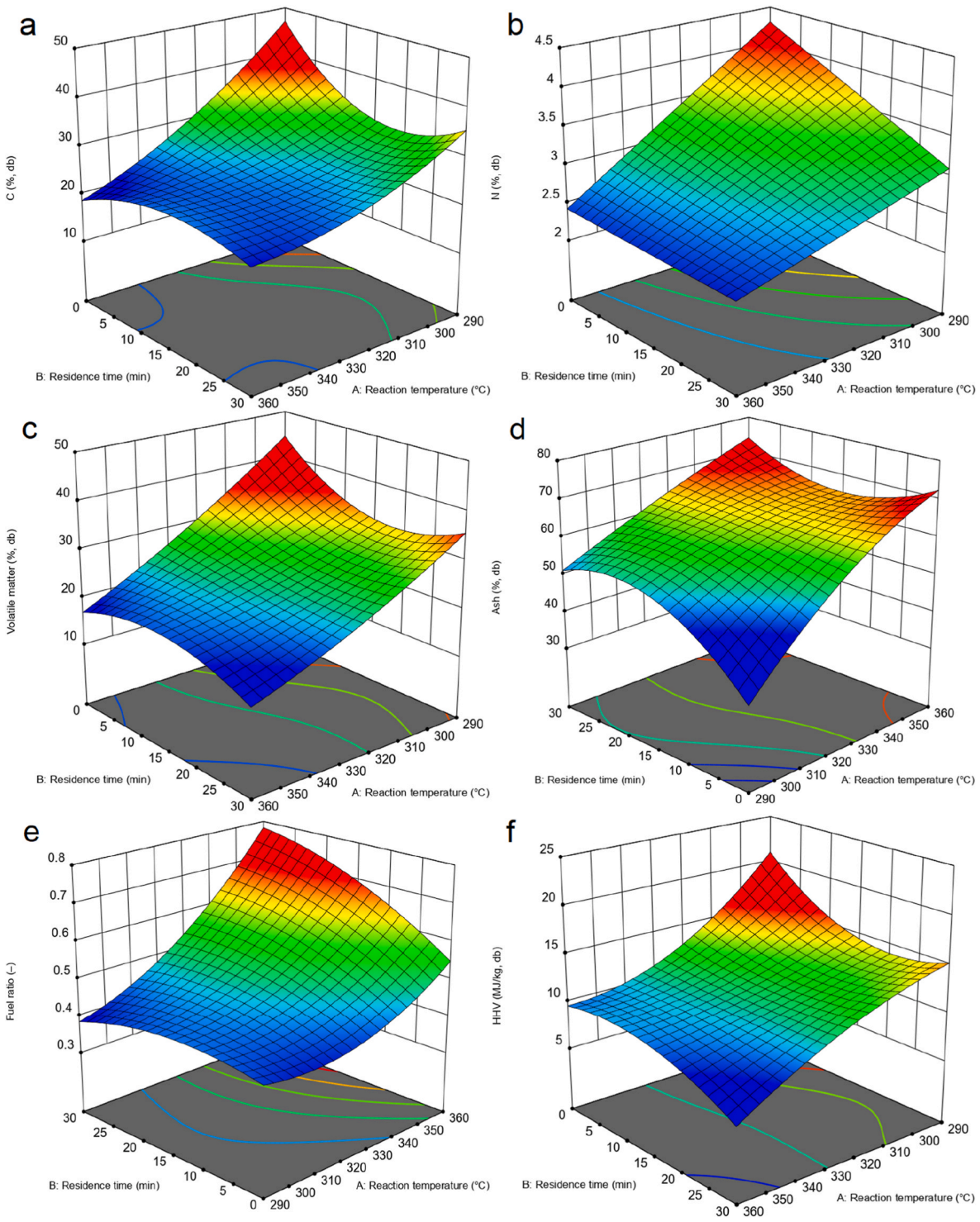

Fig. 2. Effects of HTL conditions on the contents of (a) C, (b) N, (c) volatile matter, (d) ash, (e) fuel ratio, and (f) HHV in hydrochar.

as a soil amendment.

3.1.4. Particle size distribution and surface properties

The particle sizes of hydrochar were significantly reduced compared to MS (Fig. S2). For all the hydrochar samples, 90% of particles were <113 μm (D × 90) versus 593 μm for MS, and 50% of particles were <20 μm versus 74 μm for MS (Table S4). Hydrochar obtained from different HTL conditions showed various particle size distributions. The particles dramatically downsized when increasing temperature from 290 to 325 °C, probably because of the decomposition of macromolecules (Zhuang et al., 2020). However, further raising to 360 °C generated more particles in the upper range (10–100 μm) as a result of the aggregation and cross-linking of spheres (Saha et al., 2020). HTL residence time showed similar effects to temperature on hydrochar particle size, which initially promoted small particles from 0 to 15 min and then aggregated more large particles at 30 min. The small particles of hydrochar suggested its desirability for complete combustion due to good exposure to air and suitability for nutrient extraction (particularly P) due to improved dispersibility and fast reaction rate (Liang et al., 2021).

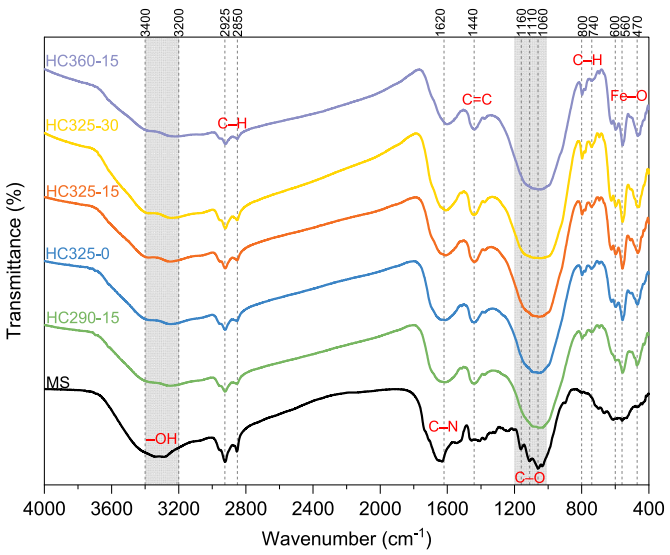

Fig. 3. FTIR spectra of MS and hydrochar from various HTL conditions.

The physisorption isotherms obtained for all MS and hydrochar samples corresponded to a reversible Type II isotherm (Fig. S3), according to the International Union of Pure and Applied Chemistry classification (Sing, 1985). This type of isotherm suggests non-porous or agglomerated samples, which was further confirmed by the SEM images (Fig. S4). The specific surface area of MS (9.14 m^2/g) and its derived hydrochar (7.39–25.17 m^2/g) were low (Table S4), as comparable to HTC (Wang et al., 2020a) and HTL hydrochar (Leng et al., 2015b) from previous studies. The surface area of hydrochar initially increased and then decreased as the temperature increased from 290 to 360 °C, while longer residence time slightly decreased the surface area. The decrease in surface area could be contributed by the cross-linking of microspheres and formation of larger particles (Saha et al., 2020). For example, increasing HTL residence time significantly enlarged the particle size of D × 10 and D × 50, which could reduce the surface area. The poor surface area and porosity indicated that subsequent modification or activation might be needed for high value-added utilization, such as adsorbent and capacitive material.

The SEM images were taken to observe the surface morphology. As shown in Fig. S4a, dried and ground MS showed diverse particle shapes for its heterogeneity. MS had a relatively smooth surface with a globular structure on the surface but no obvious pores or pathways. After HTL, the clustered aggregates (flocs and cellular tissues) of MS were transformed into small fragments in hydrochar due to the decomposition of sludge matrix. This is consistent with the particle size distribution. Unlike the hydrochar produced at a low temperature (e.g., <220 °C) that could form surface pores (Wang et al., 2020a), HTL hydrochar from a temperature above 290 °C generally did not have pores (Figs. S4b–d). It was suggested that mild reaction temperatures could dissolute substances and create porous structures, while excessive temperatures caused pores to collapse and formed irregular grooves. High temperatures also generated sphere-like aggregates in hydrochar, which were possibly composed of hydrophobic aromatic structures and hydrophilic shells from the aromatization and polymerization reactions (Wang et al., 2020b). SEM images also showed that large particles in hydrochar reduced with the increase of reaction temperature.

3.1.5. Mineral structure

XRD analysis was employed to investigate the evolution of mineral crystalline phases (Fig. S5). For MS, the diffraction peaks were simply chantalite for its low ash content. After HTL, more crystalline phases were present in hydrochar due to the accumulation of minerals, which were mainly anorthite, quartz, and some complex with alkali and alkaline earth metals (AAEMs, e.g., cordierite). Most studies also found that the major crystalline phases were silica compounds (Liu et al., 2021a, 2021b). There were no significant changes among hydrochar samples from various HTL conditions. Only slight increases in the peak intensities were observed at higher temperatures or longer residence time. However, phosphates were not detected by XRD, which could be in amorphous forms or overlapped by other phases. The presence of amorphous phosphates may favor the extraction and recovery of P as they are more unstable and soluble than the crystalline phosphates (e.g., hydroxyapatite) (Clèries et al., 1998).

3.2. Environmental impacts of hydrochar

3.2.1. Total macronutrients and COPCs

The total concentration of macro elements and COPCs were presented in Fig. 4. Compared to MS, the inorganic contents in hydrochar mostly elevated 2–10 times higher on a dry basis. Their total concentrations further increased with HTL reaction temperature and/or residence time. Notably, the mineral contents in hydrochar were directly related to the constituents of HTL feedstock (MS). Hydrochar primarily consisted of minerals in the following order: Transition metals (8.5–10.5%, db) > P (7.2–8.5%, db) > alkaline earth metals (5–5.9%, db) > post-transition metals (1.7–1.9, db) > alkali metals (0.3–0.6%, db). Particularly, hydrochar contained a large amount of Fe (8–9.8%, db), Ca (3.7–4.4%, db), Al (1.7–1.9%, db), and Mg (1.3–1.4%, db) that have strong affinities to P. It had an upper level of Fe compared to other sludge-derived hydrochar (Liu et al., 2021b), probably due to the dose of $FeCl_3$ in sewage treatment for odor control. Compared to other metals, K and Na showed lower enrichments as they were mobilized to HTL aqueous.

Fig. 4b illustrated the total heavy metals in MS and hydrochar compared to the criteria for soil amendments in BC, Canada (*B.C. Reg. 210/2007*). Similar to macronutrients, heavy metals were accumulated into hydrochar after HTL, which were ranked as: Zn (3093–4022) > Cu (1350–1641) > Cr (114–137) > Pb (94–113) > Ni (51–78) > Mo (28–37) > Se (9–9.8) > Co (5.9–6.9) > As (2.6–7.5) > Cd (1.8–4.3) > Hg (2.4–3) (unit: mg/kg, db). This rank is generally consistent with a previous study about the accumulation rate of heavy metals in hydrochar (Wang et al., 2019). Regarding total COPCs, MS was suitable for soil amendment. However, after HTL, hydrochar could be restricted from land application due to the exceedance of Zn (>1850 mg/kg) and Mo (>20 mg/kg). The long-term application of hydrochar to soil might elevate the accumulation risk of heavy metals in the food chain. It should be noted that the risk to the environment also depends on the leachability and chemical species of COPCs (Shao et al., 2015). On the other hand, the concentration of nutrients and metals in hydrochar provides opportunities for their holistic management and recycling.

3.2.2. TCLP toxicity

The TCLP simulates the leaching in landfill conditions to determine the mobility and hazardous contents of COPCs present in MS and hydrochar. Based on the preliminary tests, extraction fluid #2 (pH 4.93) was determined as the extractant. As shown in Table S5, the leachable contents of inorganic contaminants from MS and various hydrochar were well below (>100 times lower) the hazardous waste criteria in BC, Canada. Compared to MS, most COPCs (except As, Ba, B, and Zn) in hydrochar showed 10 times lower leachability. Among the examined contaminants, Zn showed the highest leachable concentration while Cd, Hg, Pb, Ag, and U had the lowest, as coherent to their total contents. Although the total COPCs in hydrochar increased with HTL reaction severities, their leachable toxicity did not raise. The reducing environment of HTL can also convert highly mobile species, e.g., Cr(VI), into immobile forms, e.g., Cr(III) in hydrochar, thus limiting the leachability and toxicity (Chen et al., 2020). The results demonstrated that HTL could alleviate the mobility and risks of heavy metals, as agreed in the literature (Liu et al., 2021a).

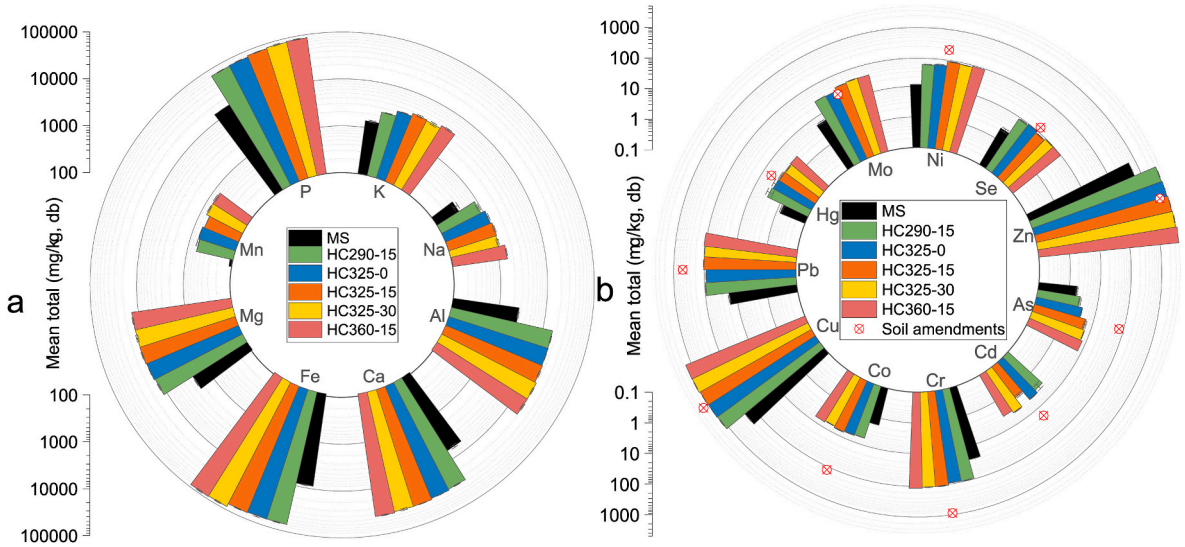

Fig. 4. Total concentrations of (a) major elements and (b) COPCs in MS and hydrochar. Cd in MS was below detection limit (<0.06 mg/kg, db).

3.2.3. pH-dependent leaching test

Apart from the total contents and leaching toxicity, it is important to evaluate the leaching behavior of COPCs under different management scenarios. The LSP test measures the leaching activities of COPCs within a wide pH range (2–13), which can provide an assessment of hydrochar in disposal, beneficial use, and treatment effectiveness. Compared to MS (5.2), hydrochar from various HTL conditions had slightly higher natural pH (5.8–5.9) values. The acid-base titration curves (Fig. 5a) showed that hydrochar had a greater acid buffering capacity (acid addition >0) than MS but a lower base buffering capacity (acid addition <0). The higher pH and acid neutralization capacity of hydrochar were probably linked to the elevated contents of AAEMs, suggesting its potential application for acidic soil amendment (Romero Millán et al., 2021). The eluate conductivity of MS and hydrochar under natural

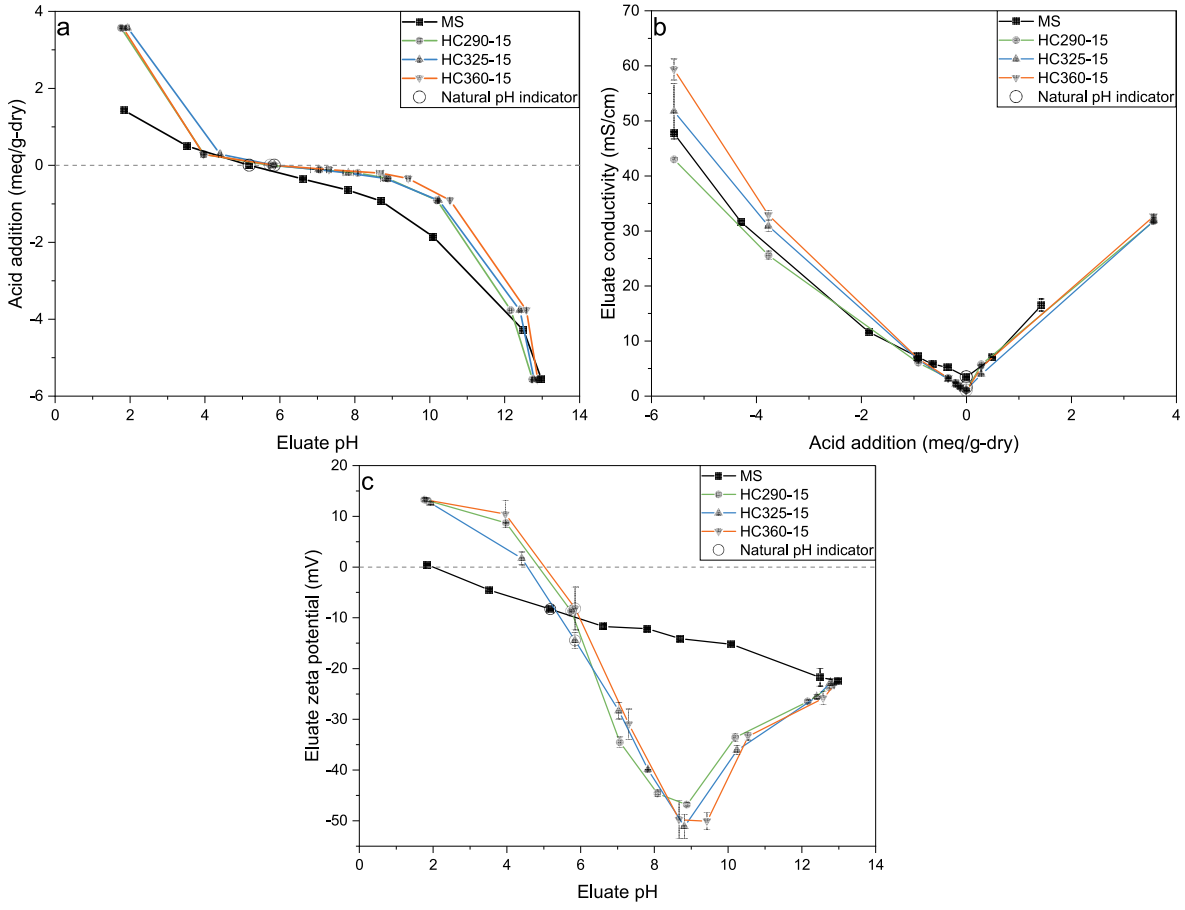

Fig. 5. (a) Acid/base addition, (b) elute conductivity, and (c) elute zeta potential of MS and hydrochar as a function of elute pH. Leaching conditions: L/S = 10 mL/g-dry, 30 rpm, 22 ± 1 °C, and 24 h.

conditions was low (<3.5 mS/cm), which increased linearly with acid/base addition (Fig. 5b). The point of zero charge (pH_{PZC}) was determined at the pH where the eluate zeta potential equals 0 (zero net charge), which was 2 and 4.6–5 for MS and hydrochar, respectively (Fig. 5c). It indicates that the surface of MS was negatively charged at all pH ranges (2–13), while hydrochar was positively charged at pH < 4.6. The negative surface charge is beneficial for retaining cations in land application.

Fig. 6 compared the partitioning of selected COPCs between MS and hydrochar, exhibiting a significant difference. Those COPCs in MS were highly soluble species as the LSP curves were weakly dependent on pH (varied within an order of magnitude at all pH), meaning that their leaching is typically related to L/S ratio. However, COPCs in hydrochar showed a strong dependence on the leaching pH. Some (e.g., As, Co, Ni, and Zn) became amphoteric species in hydrochar. The eluate content of amphoteric COPCs, such as reduced As(III) and Cr(III), displayed a U-shaped curve, which could have maximum leaching concentrations at low (2) or high (13) pH (Garrabrants et al., 2021). It should be noted that As(III) is a toxic and mobile form that requires further attention although hydrochar had limited As leaching (<1 mg/L). Multiplying the leaching content (mg/L) by 10 (L/S ratio) gives the COPC release (mg/kg), indicating almost all As could be released from MS and hydrochar at pH > 10. The other COPCs (e.g., Cr, Cu, Pb, Mo, and Se) converted partially oxidized, initially showing amphoteric behavior and then reaching the maxima at the near-alkaline pH range due to the transformation into oxyanions, e.g., Cr(VI), Mo(VI), and Se(VI). With the presence of Fe(II)/Fe(III) (cordierite) in hydrochar, the redox potential could decrease with increasing pH, thus changing the oxidation-reduction environment and metal species (Pang et al., 2007). Reducing conditions can especially favor the mobilization of As(III) and Mo. At alkaline pH, the increase of dissolved organic matter may be responsible for the higher release of some COPCs (e.g., As, Cr, Cu, Pb, Mo, and Se) through forming soluble organic complexes (Fang et al., 2016). Nevertheless, examining the valence state of COPCs would be useful to demonstrate their species, toxicity, and changes under various conditions. For Cd and Hg, their leachable contents were all below 0.1 mg/L (data not shown) due to their low total concentrations in MS and hydrochar. Overall, HTL reaction temperature (290–360 °C) did not significantly alter the leaching behaviors of COPCs. Most COPCs except for micronutrient Zn in hydrochar showed limited leachabilities (<1 mg/L) over a wide pH range (2–13), which could diminish concerns about the beneficial use of hydrochar. However, the increased maximum leaching concentration after HTL implied the potential risk of As, Mo, Ni, and Zn release. Considering the significant immobilization of most COPCs at near-neutral conditions, the applicable pH domain of hydrochar could be limited to 4–8.

3.3. *Potential applications of hydrochar*

3.3.1. *P recovery*

After HTL around 85–92% of P was recovered in hydrochar from MS regardless of the reaction conditions (Fig. 7). The total P (TP) in hydrochar gradually enhanced from 7.2%, db at 290 °C to 8.5%, db at 360 °C, compared to only 1.4%, db in MS. The P content was comparable to that in phosphate rock (11–15% P), implying that sludge-derived hydrochar could be a promising source for P recovery and recycling to mitigate environmental challenges and fulfill P demands (Liu et al., 2021b). Due to the presence of multivalent metals (e.g., Ca, Mg, Al, and Fe), P can be immobilized into various species during HTL. As shown in Fig. 7, most OP in MS (8%) was transformed into IP in hydrochar (<1%) due to the hydrolysis of poly- and organic phosphates in the microbial cells and release of orthophosphates (Wang et al., 2020a). NAIP (base-extractable) was the major P fraction in MS for the dominance of Fe, while over 30% converted into AP (acid-extractable) after HTL since calcium phosphates are more thermal-stable. The contents of NAIP and AP in hydrochar increased with reaction severities until 325 °C, whereas

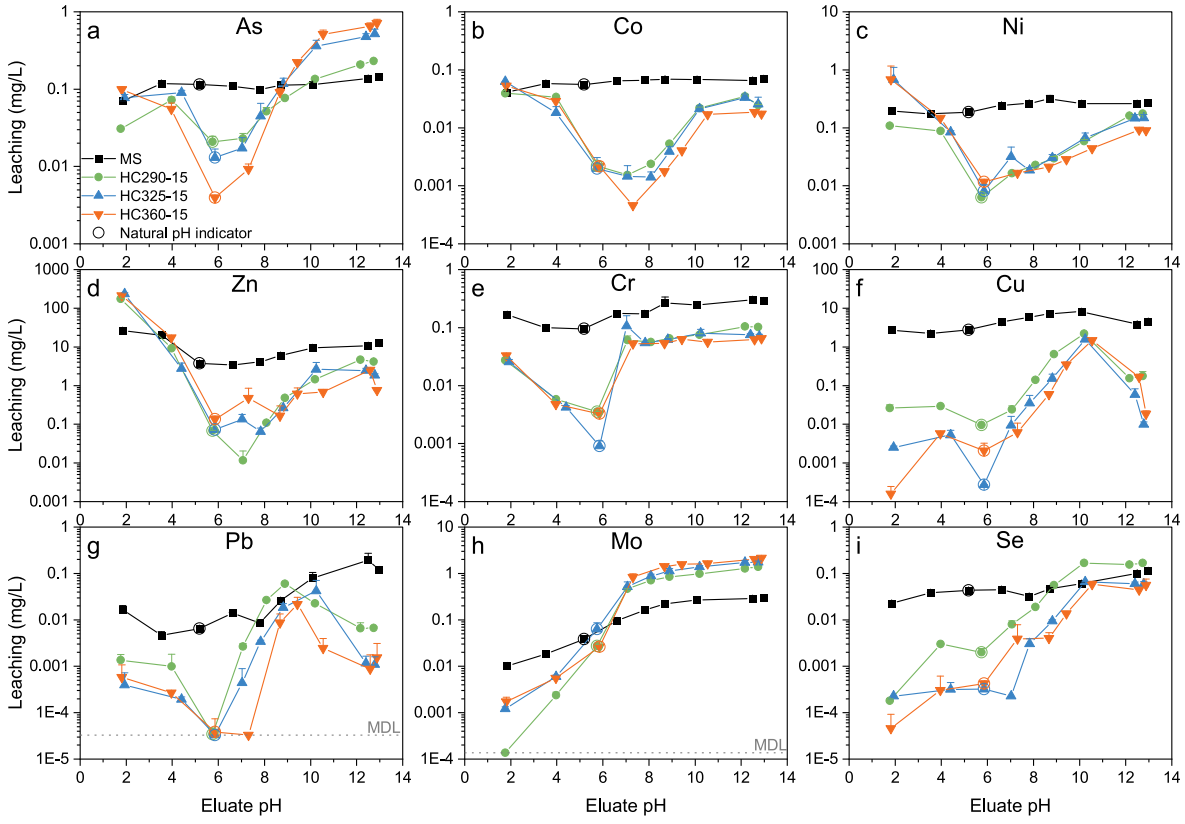

Fig. 6. Leachable contents of COPCs from MS and hydrochar as a function of elute pH. Leaching conditions: L/S = 10 mL/g-dry, 30 rpm, 22 ± 1 °C, and 24 h. MDL – method detection limit.

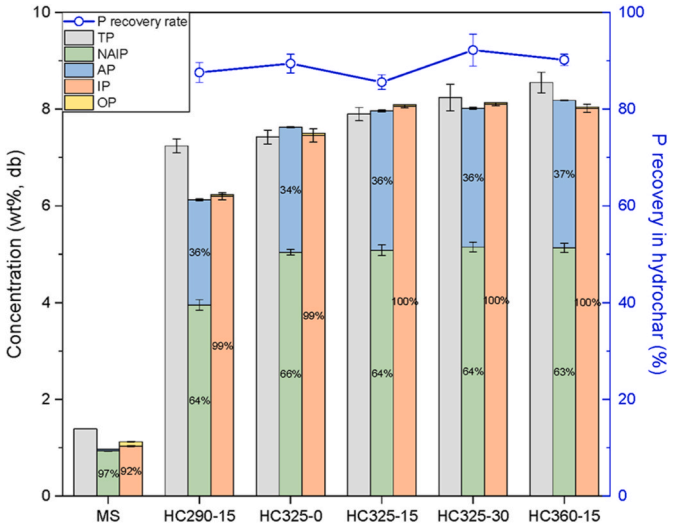

Fig. 7. P recovery rate in hydrochar from MS and P speciation in MS and hydrochar.

their relative percentages remained constant, suggesting an equilibrium condition during HTL. Notably, there was a large gap between TP and IP + OP for HC290-15, probably because a low HTL temperature generated pyrophosphate that was underestimated by the colorimetric method (Shi et al., 2019). Higher reaction severities can convert most P into orthophosphate and benefit P recovery. The current options for P recovery are mainly wet-chemical extraction and thermochemical process, whereas wet-chemical extraction is mostly applied for its cost-effectiveness (Liu et al., 2021a, 2021b). The speciation results indicated that direct alkaline extraction could be applied to recover NAIP from MS, but acidic extraction would be more suitable for P recovery from hydrochar.

From the LSP tests, the release of P and major metals as a function of pH was plotted in Fig. 8. The extraction of P from MS and hydrochar was strongly related to the elute pH. Compared to MS, P in hydrochar was less mobile, especially at pH 4–10 nearly no release. OP in MS probably contributed to a large portion of available P (Fournie et al., 2021). Although both low (2) and high (13) pH improved P release, the extraction was limited to 67% and 39% from MS and hydrochar, respectively. This suggests that more extreme conditions (pH $<$ 2 or $>$13) are necessary to extract most P. It also seemed that higher HTL temperatures (e.g., 360 °C) could constrain the release of P. Notably, the leaching behavior of P was similar to trivalent Al and Fe, whereas divalent metals (e.g., Ca, Mg, and Mn) showed much higher release at pH 2. He et al. (2020) suggested that P bound to Ca and Mg could dissolve rapidly at pH 2, and $AlPO_4$ and $FePO_4$ only dissolved partially, which can reprecipitate at pH around 2. Therefore, it was inferred that P extraction rate was mainly limited by the NAIP species, and a pH less than 2 is necessary for P recovery from hydrochar.

3.3.2. *Combustion*

Fig. 9 showed the combustion behaviors of MS and hydrochar, which can be classified into three stages: Moisture evaporation (30–150 °C), devolatilization, or volatile combustion (150–350 °C), and char or fixed carbon combustion (350–550 °C). Although hydrochar only displayed one DTG peak (Fig. 9a) in the range of 150–550 °C, the DSC curves (Fig. 9b) clearly presented two oxidation zones. Compared to MS, hydrochar can perform more stable combustion as the heat flow of MS sharply dropped after 310 °C due to its much higher volatile content than fixed carbon. The temperatures of ignition (T_i) and peak combustion rate (T_m) for hydrochar increased with HTL temperature and residence time probably due to the reduction of volatile matter and higher fuel ratio (Table S6). A high ignition point could reduce the fire and

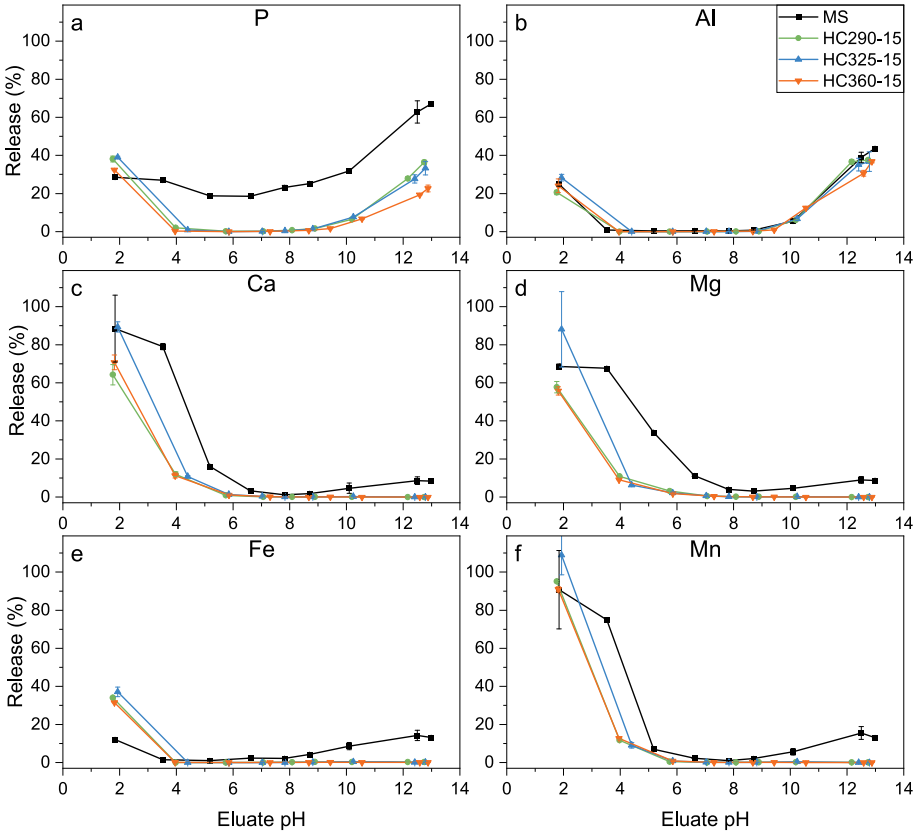

Fig. 8. Release of P and major metals from MS and hydrochar as a function of pH. Extraction conditions: L/S = 10 mL/g-dry, 30 rpm, 22 ± 1 °C, and 24 h.

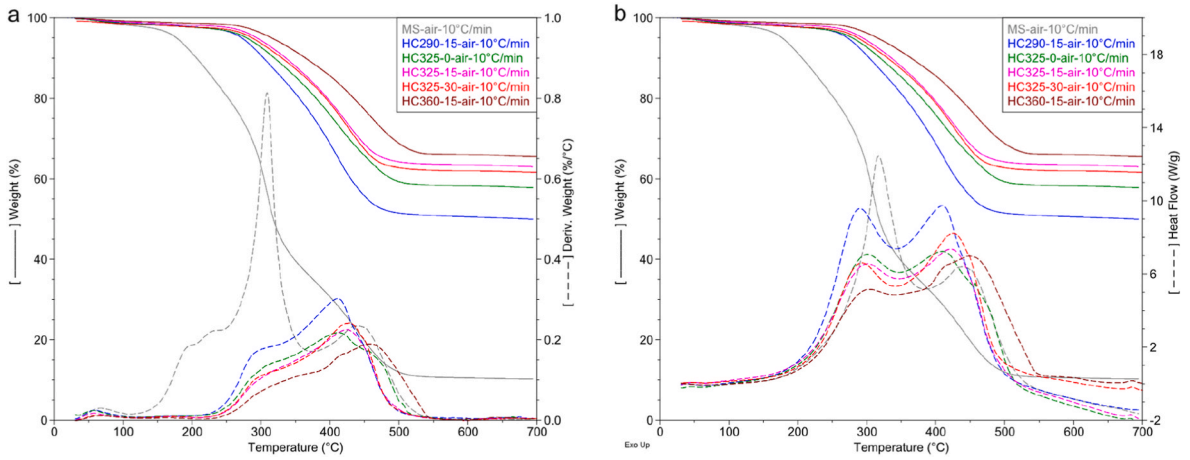

Fig. 9. TGA–DSC curves showing (a) derivative weight and (b) heat flow of MS and hydrochar.

explosion risk as a solid fuel. The burnout temperature initially declined and then increased with increasing HTL reaction severities, which might be due to the combined effects of ash and fixed carbon (He et al., 2019). The combustion index (S) dropped dramatically after HTL, suggesting inhibited combustion rate for hydrochar, which could favor stable combustion. However, the alkali index (AI) indicated that hydrochar had a slagging risk (0.17–0.34 kg/GJ), up to a virtually certain level to slag and foul (>0.34 kg/GJ) with increasing HTL temperature and residence time, compared to no risk for MS (<0.17 kg/GJ) (Miles et al., 1995). The slagging and fouling are mainly caused by the formation of alkali silicates and alkali sulfates, which can melt and deposit on combustor surfaces (Smith et al., 2016). Also considering the nutrient contents, directly burning HTL hydrochar is discouraged. Acidic extraction of hydrochar can be a sustainable solution to recover P and enhance the combustion performance of hydrochar simultaneously.

3.3.3. Carbon sequestration

The recalcitrance index (R_{50}) has been widely used to access the thermal stability and carbon sequestration potential of biochar and hydrochar (Fu et al., 2022; Harvey et al., 2012). This is an energy-based approach, meaning that a higher R_{50} suggests more high-energy carbon bonds (e.g., aromatics) and greater carbon sequestration potential. R_{50} has shown a strong correlation to H/C atomic ratio and aromaticity in hydrochar (Zhu et al., 2019). Based on R_{50}, carbon sequestration potential was divided into three classes from high to low: Class A ($R_{50} \geq 0.7$), Class B ($0.5 \leq R_{50} < 0.7$), and Class C ($R_{50} < 0.5$), with increasing biodegradability. Although hydrochar was graded as Class C, higher HTL temperatures could enhance its R_{50} up to 0.48 (HC360-15), compared to 0.35 in MS (Table S7). Notably, this classification was only based on a one-year incubation of carbon mineralization (Harvey et al., 2012), which should be refined by longer field studies. A 7-year field weathering study found that a biochar with a R_{50} around 0.5 could have a high recalcitrance (Williams et al., 2019). The high contents of alkali metals (e.g., K and Na) in hydrochar may lower $T_{50,\,HC}$ for their catalytic effects and lead to the underestimation of hydrochar recalcitrance index. Based on the O/C molar ratio, hydrochar was rated as the Class 1 biochar with a half-life of >1000 years (O/C < 0.2), while MS was categorized as Class 2 with 100–1000 years of half-life ($0.2 \leq$ O/C < 0.6) (Spokas, 2010). As a result of O removal, more stable structures, such as C═C and C═O, could be formed in hydrochar, making it less labile and turning into a more stable carbon pool (Zhu et al., 2019). The above results indicated that hydrochar could be effective for carbon sequestration with improved stability at higher HTL reaction severities.

3.3.4. Thermal upgrading to graphite by inherent catalytic metals

The conventional synthesis of graphite typically requires high temperature (2000–3000 °C) and complex procedures, which is costly for the production of well-ordered structure (Destyorini et al., 2021). The inorganics in hydrochar cause challenges for management but could be turned into a benefit for their catalytic activities, leading to a low-temperature graphitization. Through pyrolysis of hydrochar at up to 1200 °C under a nitrogen environment, DTG curves (Fig. 10) suggested the following possible graphite-forming reactions catalyzed by inherent metals (Giudicianni et al., 2021; Nzihou et al., 2013). It also indicated that reactions were delayed especially after 800 °C at a faster heating rate (30 °C/min), while the slow heating rate (10 °C/min) gave more time for catalytic reactions.

- Carbonization (750–1000 °C):

$$M_xCO_3 + 2C\ (non-graphite) \rightarrow xM + 3CO \quad (4)$$

$$M_xCO_3 \rightarrow M_xO + CO_2 \quad (5)$$

$$M_x(OH)_2 \rightarrow M_xO + H_2O \quad (6)$$

$$xM + 2H_2O \rightarrow M_x(OH)_2 + H_2 \quad (7)$$

$$M_x(OH)_2 + CO \rightarrow M_xCO_3 + H_2 + C\ (non-graphite) \quad (8)$$

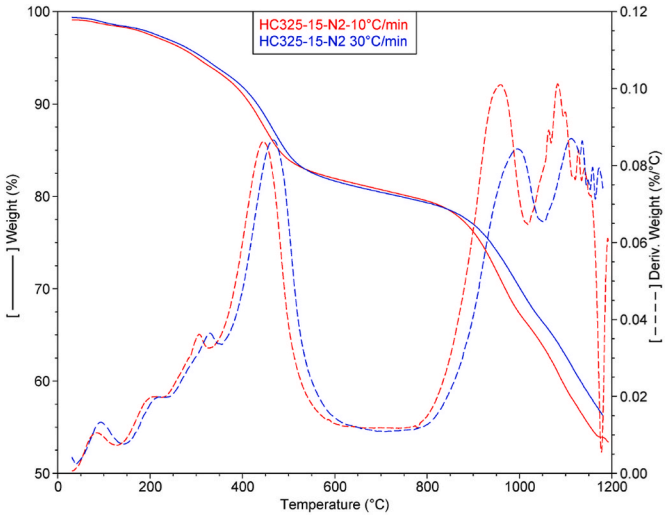

Fig. 10. TG–DTG curves for the pyrolysis of HC325-15 at a heating rate of 10 and 30 °C/min.

Graphitization (>1000 °C):

$$M_xO_y + C\ (non-graphite) \rightarrow M_xO_{y-1} + CO \rightarrow M_xO_y + C\ (graphite) \quad (9)$$

where M represents AAEMs (6.1%, db), transition metals (8.8%, db), and post-transition metals (1.8%, db).

The formation of graphitic nanostructures in hydrochar after pyrolysis was confirmed by TEM images. The low-magnification images (Fig. 11a and b) showed many dark metal nanoparticles (primarily Fe, Ca, Mg, and Al) embedded in carbon, as also demonstrated by EDX maps (Fig. 11c and d). Notably, at a faster heating rate, the carbon structure was still poorly ordered, mainly with amorphous and turbostratic phases (Fig. 11a), while only a little graphite-like material (in red square) was identified around the metal particles. However, the slow heating rate (10 °C/min) generated much better-ordered carbon structures (Fig. 11b), with large ribbons of straight stacked graphitic layers found both passing through and around the metal particles. After the fast Fourier transform using DigitalMicrograph® (version 3.5), the interplanar distance (d) of graphitic layers was estimated at 0.331 and 0.336 nm for hydrochar pyrolyzed at 30 and 10 °C/min, respectively. These values were consistent with the inter-graphene spacing (0.33–0.37 nm) from the literature (Mubari et al., 2022). The interplanar spacing of metals near graphite layers was 0.203–0.206 nm, which was likely the

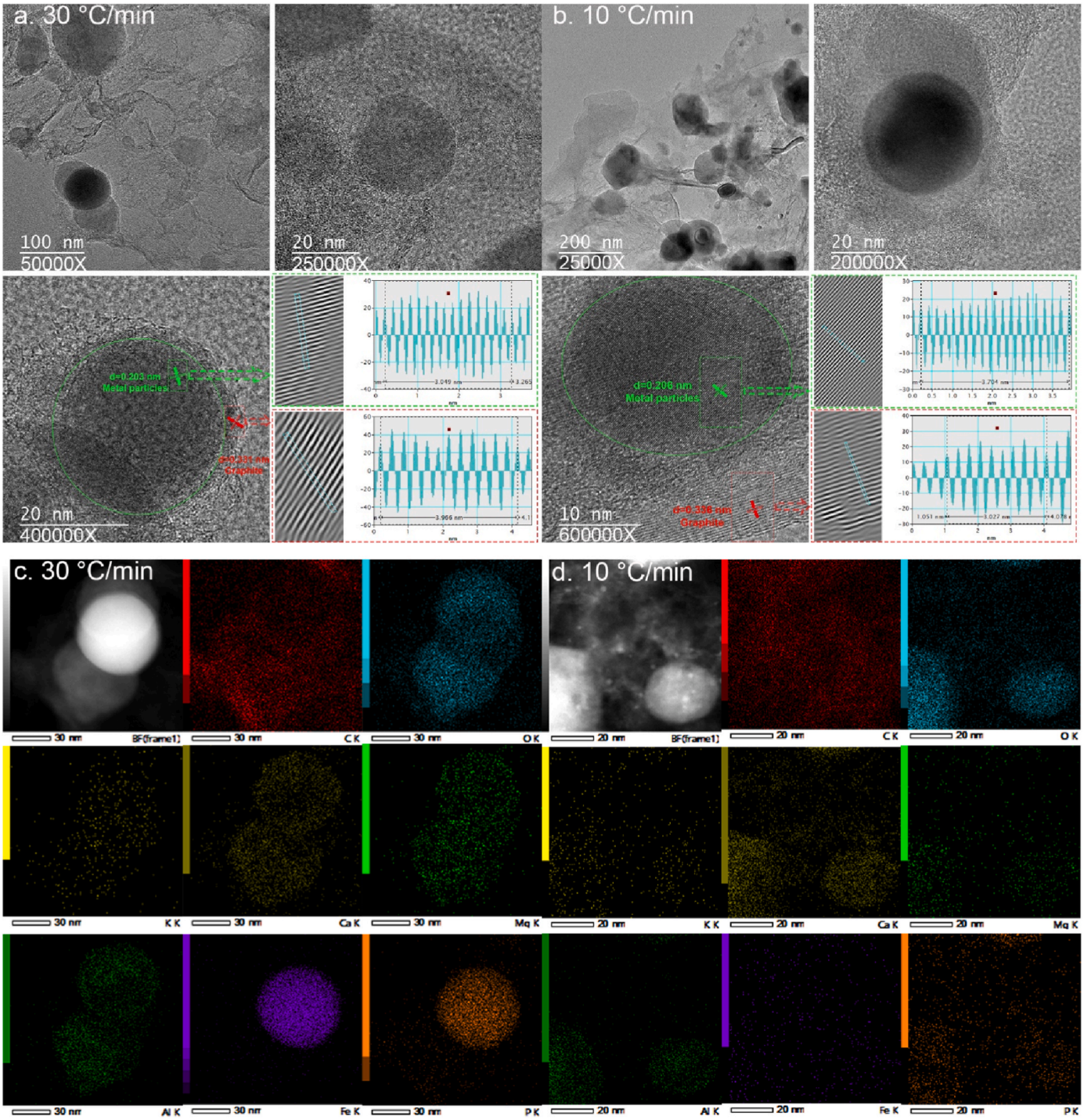

Fig. 11. TEM (a–b) and EDX (c–d) images of HC325-15 after pyrolysis at a heating rate of 30 and 10 °C/min.

lattice plane of Fe(110) (Li et al., 2015). Noticeably, the metal-catalyzed graphitization was favored at a low heating rate or long reaction time. Using hydrochar for graphite production was rarely reported to date, while this study has proved its potential for catalytic graphitization by inherent metals. Indeed, the process requires further investigation and optimization to improve graphite purity. Alternatively, hydrochar may be dosed as a catalyst for graphitization considering its high mineral contents.

4. Conclusion

After the comprehensive assessment of characteristics, environmental impacts, and possible utilizations of HTL hydrochar, this study concluded with the following remarks:

- The remaining solid residue (hydrochar) was significantly reduced to $\leq$3.5 wt% (wet basis) for minimal disposal cost. With increasing HTL reaction severities, hydrochar contained lower contents of volatile matter, CHNSO, HHV, O/C, and H/C but higher ash and fuel ratio. It also showed the decreased intensity of oxygenated groups and enhanced intensity of aromatic groups compared to MS. The significant reduction of particle size ($D \times 90 < 113$ μm) in hydrochar could favor its application. The limited porosity and surface area (7.39–25.17 m^2/g) may restrict its adsorption capacity and thus require activation.
- Compared to MS, total concentrations of COPCs in hydrochar drastically increased (up to 10 times), thus restricting the direct land application. However, the TCLP toxicity of most COPCs dropped 10 times. Most COPCs (except Zn) in hydrochar had limited leachabilities (<1 mg/L) at pH 2–13. The overall leaching risk of COPCs in hydrochar was controlled. However, the identification of aromatic and N-containing groups suggested that studies about potential toxic organic compounds (e.g., dissolved organic matter and N-heterocycles) are necessary for the holistic risk management of hydrochar.
- Hydrochar is promising for various applications. It is gifted for P recovery with a TP (7.2–8.5%, db) comparable to phosphate rock, and acidic extraction (pH < 2) would be feasible for P recovery due to high AP contents (>34%). It is a good candidate for carbon sequestration due to improved carbon stability and recalcitrance. The substantial content of metals (e.g., Ca and Fe) in hydrochar could deliver promising catalytic graphitization at a low temperature (1200 °C). Hydrochar also exhibited more stable combustion performance than MS but required ash removal to mitigate the risk of ash slagging and fouling.

CRediT authorship contribution statement

Huan Liu: Conceptualization, Data curation, Formal analysis, Investigation, Methodology, Software, Validation, Visualization, Writing – original draft. **Nathalie Lyczko:** Data curation, Resources, Writing – review & editing. **Ange Nzihou:** Supervision, Writing – review & editing. **Cigdem Eskicioglu:** Conceptualization, Funding acquisition, Project administration, Resources, Supervision, Writing – review & editing.

Declaration of competing interest

The authors declare that they have no known competing financial interests or personal relationships that could have appeared to influence the work reported in this paper.

Data availability

Data will be made available on request.

Acknowledgments

This research was funded by the program of Natural Sciences and Engineering Research Council of Canada (NSERC)/Metro Vancouver Industrial Research Chair in Advanced Resource Recovery from Wastewater, Canada (IRCPJ 548816-18). The authors are thankful to the anonymous reviewers for improving this article.

Appendix A. Supplementary data

Supplementary data to this article can be found online at https://doi.org/10.1016/j.jclepro.2022.135398.

References

Basar, I.A., Liu, H., Carrere, H., Trably, E., Eskicioglu, C., 2021. A review on key design and operational parameters to optimize and develop hydrothermal liquefaction of biomass for biorefinery applications. Green Chem. 23, 1404–1446. https://doi.org/10.1039/D0GC04092D.

Chang, Y., Xiao, X.-F., Huang, H., Xiao, Y.-D., Fang, H.-S., He, J.-B., Zhou, C.-H., 2021. Transformation characteristics of polycyclic aromatic hydrocarbons during hydrothermal liquefaction of sewage sludge. J. Supercrit. Fluids 170, 105158. https://doi.org/10.1016/j.supflu.2020.105158.

Chen, H., Zhai, Y., Xu, B., Xiang, B., Zhu, L., Qiu, L., Liu, X., Li, C., Zeng, G., 2014. Fate and risk assessment of heavy metals in residue from co-liquefaction of Camellia oleifera cake and sewage sludge in supercritical ethanol. Bioresour. Technol. 167, 578–581. https://doi.org/10.1016/j.biortech.2014.06.048.

Chen, Y., Chen, H., Thring, R.W., Liu, H., Zhou, J., Tao, Y., Li, J., 2020. Immobilization of chromium contaminated soil by Co-pyrolysis with rice straw. Water, air. Soil Pollut 231, 200. https://doi.org/10.1007/s11270-020-04581-3.

Clèries, L., Fernández-Pradas, J.M., Sardin, G., Morenza, J.L., 1998. Dissolution behaviour of calcium phosphate coatings obtained by laser ablation. Biomaterials 19, 1483–1487. https://doi.org/10.1016/S0142-9612(98)00063-5.

Destyorini, F., Yudianti, R., Irmawati, Y., Hardiansyah, A., Hsu, Y.I., Uyama, H., 2021. Temperature driven structural transition in the nickel-based catalytic graphitization of coconut coir. Diam. Relat. Mater. 117, 108443 https://doi.org/10.1016/j.diamond.2021.108443.

Devi, P., Liu, H., Basar, I.A., Eskicioglu, C., 2022. Value-added hydrochar recovery from anaerobic digestate for environmental applications. In: Anaerobic Digestate Management. IWA Publishing, pp. 189–224. https://doi.org/10.2166/9781789062755_0189.

Đurđević, D., Blecich, P., Jurić, Ž., 2019. Energy recovery from sewage sludge: the case study of Croatia. Energies 12, 1927. https://doi.org/10.3390/en12101927.

Fang, W., Wei, Y., Liu, J., 2016. Comparative characterization of sewage sludge compost and soil: heavy metal leaching characteristics. J. Hazard Mater. 310, 1–10. https://doi.org/10.1016/j.jhazmat.2016.02.025.

Fournie, T., Switzer, C., Gerhard, J.I., 2021. USEPA LEAF methods for characterizing phosphorus and potentially toxic elements in raw and thermally treated sewage sludge. Chemosphere 275, 130081. https://doi.org/10.1016/j.chemosphere.2021.130081.

Fu, H., Wang, B., Wang, H., Liu, H., Xie, H., Han, L., Wang, N., Sun, X., Feng, Y., Xue, L., 2022. Assessment of livestock manure-derived hydrochar as cleaner products: insights into basic properties, nutrient composition, and heavy metal content. J. Clean. Prod. 330, 129820 https://doi.org/10.1016/j.jclepro.2021.129820.

Garrabrants, A.C., Kosson, D.S., Brown, K.G., Fagnant, D.P., Helms, G., Thorneloe, S.A., 2021. Demonstration of the use of test results from the Leaching Environmental Assessment Framework (LEAF) to develop screening-level leaching assessments. Waste Manag. 121, 226–236. https://doi.org/10.1016/j.wasman.2020.12.016.

Giudicianni, P., Gargiulo, V., Grottola, C.M., Alfè, M., Ferreiro, A.I., Mendes, M.A.A., Fagnano, M., Ragucci, R., 2021. Inherent metal elements in biomass pyrolysis: a review. Energy Fuel. 35, 5407–5478. https://doi.org/10.1021/acs.energyfuels.0c04046.

González Medeiros, J.J., Pérez Cid, B., Fernández Gómez, E., 2005. Analytical phosphorus fractionation in sewage sludge and sediment samples. Anal. Bioanal. Chem. 381, 873–878. https://doi.org/10.1007/s00216-004-2989-z.

Harvey, O.R., Kuo, L.J., Zimmerman, A.R., Louchouarn, P., Amonette, J.E., Herbert, B.E., 2012. An index-based approach to assessing recalcitrance and soil carbon sequestration potential of engineered black carbons (biochars). Environ. Sci. Technol. 46, 1415–1421. https://doi.org/10.1021/es2040398.

He, C., Zhang, Z., Ge, C., Liu, W., Tang, Y., Zhuang, X., Qiu, R., 2019. Synergistic effect of hydrothermal co-carbonization of sewage sludge with fruit and agricultural wastes on hydrochar fuel quality and combustion behavior. Waste Manag. 100, 171–181. https://doi.org/10.1016/j.wasman.2019.09.018.

He, C., Zhao, J., Yang, Y., Wang, J.Y., 2016. Multiscale characteristics dynamics of hydrochar from hydrothermal conversion of sewage sludge under sub- and near-critical water. Bioresour. Technol. 211, 486–493. https://doi.org/10.1016/j.biortech.2016.03.110.

He, P., Zhang, X., Lü, F., Shao, L., Zhang, H., 2020. Leaching behavior of phosphorous compounds from sewage sludge ash based on quantitative X-ray diffraction analysis. Waste Dispos. Sustain. Energy 2, 113–125. https://doi.org/10.1007/s42768-020-00037-w.

Heracleous, E., Vassou, M., Lappas, A.A., Rodriguez, J.K., Chiaberge, S., Bianchi, D., 2022. Understanding the upgrading of sewage sludge-derived hydrothermal liquefaction biocrude via advanced characterization. Energy Fuel. 36, 12010–12020. https://doi.org/10.1021/acs.energyfuels.2c01746.

Huang, H., Yuan, X., Zeng, G., Zhu, H., Li, H., Liu, Z., Jiang, H., Leng, L., Bi, W., 2011. Quantitative evaluation of heavy metals' pollution hazards in liquefaction residues of sewage sludge. Bioresour. Technol. 102, 10346–10351. https://doi.org/10.1016/j.biortech.2011.08.117.

Johnson, G.R., 2022. PFAS in soil and groundwater following historical land application of biosolids. Water Res. 211, 118035 https://doi.org/10.1016/j.watres.2021.118035.

Kim, D., Lee, K., Park, K.Y., 2014. Hydrothermal carbonization of anaerobically digested sludge for solid fuel production and energy recovery. Fuel 130, 120–125. https://doi.org/10.1016/j.fuel.2014.04.030.

Kurose, R., Ikeda, M., Makino, H., Kimoto, M., Miyazaki, T., 2004. Pulverized coal combustion characteristics of high-fuel-ratio coals. Fuel 83, 1777–1785. https://doi.org/10.1016/j.fuel.2004.02.021.

Lachos-Perez, D., César Torres-Mayanga, P., Abaide, E.R., Zabot, G.L., De Castilhos, F., 2022. Hydrothermal carbonization and Liquefaction: differences, progress, challenges, and opportunities. Bioresour. Technol. 343 https://doi.org/10.1016/j.biortech.2021.126084.

Leng, L., Yuan, X., Huang, H., Jiang, H., Chen, X., Zeng, G., 2014. The migration and transformation behavior of heavy metals during the liquefaction process of sewage sludge. Bioresour. Technol. 167, 144–150. https://doi.org/10.1016/j.biortech.2014.05.119.

Leng, L., Yuan, X., Huang, H., Shao, J., Wang, H., Chen, X., Zeng, G., 2015a. Bio-char derived from sewage sludge by liquefaction: characterization and application for dye adsorption. Appl. Surf. Sci. 346, 223–231. https://doi.org/10.1016/j.apsusc.2015.04.014.

Leng, L.J., Yuan, X.Z., Huang, H.J., Wang, H., Wu, Z. Bin, Fu, L.H., Peng, X., Chen, X.H., Zeng, G.M., 2015b. Characterization and application of bio-chars from liquefaction of microalgae, lignocellulosic biomass and sewage sludge. Fuel Process. Technol. 129, 8–14. https://doi.org/10.1016/j.fuproc.2014.08.016.

Li, J., Wen, W., Xu, G., Zou, M., Huang, Z., Guan, L., 2015. Fe-added Fe3C carbon nanofibers as anode for Li ion batteries with excellent low-temperature performance. Electrochim. Acta 153, 300–305. https://doi.org/10.1016/j.electacta.2014.12.008.

Li, S., Jiang, Y., Snowden-Swan, L.J., Askander, J.A., Schmidt, A.J., Billing, J.M., 2021. Techno-economic uncertainty analysis of wet waste-to-biocrude via hydrothermal liquefaction. Appl. Energy 283, 116340. https://doi.org/10.1016/j.apenergy.2020.116340.

Liang, S., Yang, L., Chen, H., Yu, W., Tao, S., Yuan, S., Xiao, K., Hu, J., Hou, H., Liu, B., Yang, J., 2021. Phosphorus recovery from incinerated sewage sludge ash (ISSA) and reutilization of residues for sludge pretreated by different conditioners. Resour. Conserv. Recycl. 169, 105524 https://doi.org/10.1016/j.resconrec.2021.105524.

Liu, H., Basar, I.A., Lyczko, N., Nzihou, A., Eskicioglu, C., 2022. Incorporating hydrothermal liquefaction into wastewater treatment – Part I: process optimization for energy recovery and evaluation of product distribution. Chem. Eng. J. 449, 137838 https://doi.org/10.1016/j.cej.2022.137838.

Liu, H., Basar, I.A., Nzihou, A., Eskicioglu, C., 2021a. Hydrochar derived from municipal sludge through hydrothermal processing: a critical review on its formation, characterization, and valorization. Water Res. 199, 117186 https://doi.org/10.1016/j.watres.2021.117186.

Liu, H., Hu, G., Basar, I.A., Li, J., Lyczko, N., Nzihou, A., Eskicioglu, C., 2021b. Phosphorus recovery from municipal sludge-derived ash and hydrochar through wet-chemical technology: a review towards sustainable waste management. Chem. Eng. J. 417, 129300 https://doi.org/10.1016/j.cej.2021.129300.

Lu, J.J., Chen, W.H., 2015. Investigation on the ignition and burnout temperatures of bamboo and sugarcane bagasse by thermogravimetric analysis. Appl. Energy 160, 49–57. https://doi.org/10.1016/j.apenergy.2015.09.026.

Marrone, P.A., Elliott, D.C., Billing, J.M., Hallen, R.T., Hart, T.R., Kadota, P., Moeller, J. C., Randel, M.A., Schmidt, A.J., 2018. Bench-scale evaluation of hydrothermal processing technology for conversion of wastewater solids to fuels. Water Environ. Res. 90, 329–342. https://doi.org/10.2175/106143017x15131012152861.

Miles, T.R., Miles, T.R.J., Baxter, L.L., Bryers, R.W., Jenkins, B.M., Oden, L.L., 1995. Alkali Deposits Found in Biomass Power Plants: A Preliminary Investigation of Their Extent and Nature, ume 1. https://doi.org/10.2172/251288. Washington, DC (United States).

Mubari, P.K., Beguerie, T., Monthioux, M., Weiss-Hortala, E., Nzihou, A., Puech, P., 2022. The X-ray, Raman and TEM signatures of cellulose-derived carbons explained. Chimia 8, 4. https://doi.org/10.3390/c8010004.

Nzihou, A., 2020. Handbook on Characterization of Biomass, Biowaste and Related By-Products, Handbook on Characterization of Biomass, Biowaste and Related By-Products. https://doi.org/10.1007/978-3-030-35020-8.

Nzihou, A., Stanmore, B., Sharrock, P., 2013. A review of catalysts for the gasification of biomass char, with some reference to coal. Energy 58, 305–317. https://doi.org/10.1016/j.energy.2013.05.057.

Pang, S.C., Chin, S.F., Anderson, M.A., 2007. Redox equilibria of iron oxides in aqueous-based magnetite dispersions: effect of pH and redox potential. J. Colloid Interface Sci. 311, 94–101. https://doi.org/10.1016/j.jcis.2007.02.058.

Romero Millán, L.M., Sierra Vargas, F.E., Nzihou, A., 2021. Characterization of steam gasification biochars from lignocellulosic agrowaste towards soil applications. Waste Biomass Valorization 12, 4141–4155. https://doi.org/10.1007/s12649-020-01241-9.

Saha, N., McGaughy, K., Reza, M.T., 2020. Elucidating hydrochar morphology and oxygen functionality change with hydrothermal treatment temperature ranging from subcritical to supercritical conditions. J. Anal. Appl. Pyrolysis 152, 104965. https://doi.org/10.1016/j.jaap.2020.104965.

Sezer, S., Kartal, F., Özveren, U., 2021. The investigation of co-combustion process for synergistic effects using thermogravimetric and kinetic analysis with combustion index. Therm. Sci. Eng. Prog. 23, 100889 https://doi.org/10.1016/j.tsep.2021.100889.

Shao, J., Yuan, X., Leng, L., Huang, H., Jiang, L., Wang, H., Chen, X., Zeng, G., 2015. The comparison of the migration and transformation behavior of heavy metals during pyrolysis and liquefaction of municipal sewage sludge, paper mill sludge, and slaughterhouse sludge. Bioresour. Technol. 198, 16–22. https://doi.org/10.1016/j.biortech.2015.08.147.

Shi, Y., Luo, G., Rao, Y., Chen, H., Zhang, S., 2019. Hydrothermal conversion of dewatered sewage sludge: focusing on the transformation mechanism and recovery of phosphorus. Chemosphere 228, 619–628. https://doi.org/10.1016/j.chemosphere.2019.04.109.

Silva Thomsen, L.B., Anastasakis, K., Biller, P., 2022. Wet oxidation of aqueous phase from hydrothermal liquefaction of sewage sludge. Water Res. 209 https://doi.org/10.1016/j.watres.2021.117863.

Silva Thomsen, L.B., Carvalho, P.N., dos Passos, J.S., Anastasakis, K., Bester, K., Biller, P., 2020. Hydrothermal liquefaction of sewage sludge; energy considerations and fate of micropollutants during pilot scale processing. Water Res. 183, 116101 https://doi.org/10.1016/j.watres.2020.116101.

Sing, K.S.W., 1985. Reporting physisorption data for gas/solid systems with special reference to the determination of surface area and porosity (Recommendations 1984). Pure Appl. Chem. 57, 603–619. https://doi.org/10.1351/pac198557040603.

Smith, A.M., Singh, S., Ross, A.B., 2016. Fate of inorganic material during hydrothermal carbonisation of biomass: influence of feedstock on combustion behaviour of hydrochar. Fuel 169, 135–145. https://doi.org/10.1016/j.fuel.2015.12.006.

Spokas, K.A., 2010. Review of the stability of biochar in soils: predictability of O:C molar ratios. Carbon Manag. 1, 289–303. https://doi.org/10.4155/cmt.10.32.

Tasca, A.L., Puccini, M., Gori, R., Corsi, I., Galletti, A.M.R., Vitolo, S., 2019. Hydrothermal carbonization of sewage sludge: a critical analysis of process severity, hydrochar properties and environmental implications. Waste Manag. 93, 1–13. https://doi.org/10.1016/j.wasman.2019.05.027.

Tong, Y., Yang, T., Li, B., Kai, X., Li, R., 2021. Two-stage liquefaction of sewage sludge in methanol-water mixed solvents with low-medium temperature. J. Supercrit. Fluids 168, 105094. https://doi.org/10.1016/j.supflu.2020.105094.

Wang, H., Yang, Z., Li, X., Liu, Y., 2020a. Distribution and transformation behaviors of heavy metals and phosphorus during hydrothermal carbonization of sewage sludge. Environ. Sci. Pollut. Res. 27, 17109–17122. https://doi.org/10.1007/s11356-020-08098-4.

Wang, L., Chang, Y., Liu, Q., 2019. Fate and distribution of nutrients and heavy metals during hydrothermal carbonization of sewage sludge with implication to land application. J. Clean. Prod. 225, 972–983. https://doi.org/10.1016/j.jclepro.2019.03.347.

Wang, P., Sakhno, Y., Adhikari, S., Peng, H., Jaisi, D., Soneye, T., Higgins, B., Wang, Q., 2021a. Effect of ammonia removal and biochar detoxification on anaerobic digestion of aqueous phase from municipal sludge hydrothermal liquefaction. Bioresour. Technol. 326, 124730 https://doi.org/10.1016/j.biortech.2021.124730.

Wang, P., Tyndall, S., Rahman, T., Roy, P., Jahromi, H., Adhikari, S., Boersma, M., 2022. Sorption and recovery of phenolic compounds from aqueous phase of sewage sludge hydrothermal liquefaction using bio-char. Chemosphere 287, 131934. https://doi.org/10.1016/j.chemosphere.2021.131934.

Wang, R., Lei, H., Liu, S., Ye, X., Jia, J., Zhao, Z., 2021b. The redistribution and migration mechanism of nitrogen in the hydrothermal co-carbonization process of sewage sludge and lignocellulosic wastes. Sci. Total Environ. 776, 145922 https://doi.org/10.1016/j.scitotenv.2021.145922.

Wang, W., Chen, W.H., Jang, M.F., 2020b. Characterization of hydrochar produced by hydrothermal carbonization of organic sludge. Futur. Cities Environ. 6, 1–10. https://doi.org/10.5334/fce.102.

Watson, J., Wang, T., Si, B., Chen, W.T., Aierzhati, A., Zhang, Y., 2020. Valorization of hydrothermal liquefaction aqueous phase: pathways towards commercial viability. Prog. Energy Combust. Sci. 77, 100819 https://doi.org/10.1016/j.pecs.2019.100819.

Williams, E.K., Jones, D.L., Sanders, H.R., Benitez, G.V., Plante, A.F., 2019. Effects of 7 years of field weathering on biochar recalcitrance and solubility. Biochar 1, 237–248. https://doi.org/10.1007/s42773-019-00026-1.

Yu, Y., Yang, X., Lei, Z., Yu, R., Shimizu, K., Chen, N., Feng, C., Zhang, Z., 2019. Effects of three macroelement cations on P mobility and speciation in sewage sludge derived hydrochar by using hydrothermal treatment. Bioresour. Technol. Reports 7, 100231. https://doi.org/10.1016/j.biteb.2019.100231.

Yuan, X., Huang, H., Zeng, G., Li, H., Wang, J., Zhou, C., Zhu, H., Pei, X., Liu, Zhifeng, Liu, Zhantao, 2011. Total concentrations and chemical speciation of heavy metals in liquefaction residues of sewage sludge. Bioresour. Technol. 102, 4104–4110. https://doi.org/10.1016/j.biortech.2010.12.055.

Zhang, H., Xue, G., Chen, H., Li, X., 2018. Magnetic biochar catalyst derived from biological sludge and ferric sludge using hydrothermal carbonization: preparation, characterization and its circulation in Fenton process for dyeing wastewater

treatment. Chemosphere 191, 64–71. https://doi.org/10.1016/j.chemosphere.2017.10.026.

Zhu, X., Liu, Y., Li, L., Shi, Q., Hou, J., Zhang, R., Zhang, S., Chen, J., 2019. Nonthermal air plasma dehydration of hydrochar improves its carbon sequestration potential and dissolved organic matter molecular characteristics. Sci. Total Environ. 659, 655–663. https://doi.org/10.1016/j.scitotenv.2018.12.399.

Zhuang, X., Song, Y., Zhan, H., Yin, X., Wu, C., 2020. Influences of microstructural alternations and inorganic catalysis on the thermochemical conversion of biowaste-derived hydrochar. Fuel Process. Technol. 199, 106304 https://doi.org/10.1016/j.fuproc.2019.106304.